31
JAERI-RESEARCH-98-032
SEP 16 1998
Fermilab Library
0 1160 0067551 4

JAERI-Research
98-032

MEASUREMENT AND THEORETICAL ANALYSIS OF NEUTRON-INDUCED NEUTRON-EMISSION REACTIONS OF ^{6}Li AT 10 TO 20 MeV REGION

June 1998

DATE | M.S.
RETURN TO FERMILAB LIBRARY

Masanobu IBARAKI*, Mamoru BABA*, Shigeo MATSUYAMA*, Satoshi CHIBA,
Ko TOGASAKI**, Keiichi SHIBATA, Osamu IWAMOTO,
Arjan J. KONING*3, Gerry M. HALE*4 and Mark B. CHADWICK*4

日本原子力研究所
Japan Atomic Energy Research Institute

本レポートは，日本原子力研究所が不定期に公刊している研究報告書です。
入手の問合わせは，日本原子力研究所研究情報部研究情報課（〒319-1195　茨城県那珂郡東海村）あて，お申し越しください。なお，このほかに財団法人原子力弘済会資料センター（〒319-1195　茨城県那珂郡東海村日本原子力研究所内）で複写による実費頒布をおこなっております。

This report is issued irregularly.
Inquiries about availability of the reports should be addressed to Research Information Division, Department of Intellectual Resources, Japan Atomic Energy Research Institute, Tokai-mura, Naka-gun, Ibaraki-ken, 319-1195, Japan.

© Japan Atomic Energy Research Institute, 1998

編集兼発行　　日本原子力研究所

JAERI-Research 98-032

Measurement and Theoretical Analysis of Neutron-induced Neutron-emission Reactions of ^{6}Li at 10 to 20 MeV Region

Masanobu IBARAKI*, Mamoru BABA*, Shigeo MATSUYAMA*, Satoshi CHIBA+,
Ko TOGASAKI**, Keiichi SHIBATA, Osamu IWAMOTO,
Arjan J. KONING*3, Gerry M. HALE*4 and Mark B. CHADWICK*4

Department of Nuclear Energy System
Tokai Research Establishment
Japan Atomic Energy Research Institute
Tokai-mura, Naka-gun, Ibaraki-ken

(Received May 22, 1998)

We have measured the neutron elastic and inelastic scattering double-differential cross sections of ^{6}Li at incident neutron energies of 11.5, 14.1 and 18.0 MeV. Based on this data, together with information from other works, a phenomenological neutron optical model potential (OMP) of ^{6}Li was constructed to describe the total and elastic scattering cross sections from 5 MeV to several tens MeV. This potential also describes well the inelastic scattering to the 1st excited state (E_x=2.186 MeV) via the DWBA calculation with the macroscopic vibrational model. The continuum neutron energy spectra and angular distributions were then analyzed by the theory of final-state interaction extended to the DWBA form, with the assumption that the d- α interaction is dominant in the 3-body final state consisting of n, d and α particles. Such a calculation was found to be successful in explaining the major part of the low-excitation neutron spectra and angular distribution down to the Q-value region of -9 MeV, except for the Q-value range where the n- α quasi-free scattering will give a non-negligible contribution at forward angles.

Keywords: ^{6}Li(n,n) and (n,n')d α Reactions, Neutron Emission, Double-differential Cross Sections, Optical Model, DWBA, Final-state Interaction

+ Advanced Science Research Center
* Tohoku University
** Science and Technology Agency
*3 Netherlands Energy Research Foundation ECN
*4 Los Alamos National Laboratory

10から20MeV領域における^{6}Liの中性子入射による中性子放出反応の測定及び理論解析

日本原子力研究所東海研究所エネルギーシステム研究部
茨木　正信*・馬場　護*・松山　成男*・千葉　敏+
戸ケ崎　康**・柴田　恵一・岩本　修・Arjan J. KONING*3
Gerry M. HALE*4・Mark B. CHADWICK*4

(1998年5月22日受理)

入射中性子エネルギー11.5、14.1及び18.0 MeVにおける^{6}Liからの中性子放出反応の二重微分断面積を測定した。このデータ及び他の測定により得られたデータを基に、^{6}Liの中性子全断面積と弾性散乱の角度分布を5 MeVから数10 MeVにわたるエネルギー領域で再現できる光学ポテンシャルを構築した。このポテンシャルは、DWBA理論による計算を通して、第一励起準位（励起エネルギー2.186 MeV)への非弾性散乱の角度分布をも良く再現できることが分かった。次に、連続状態への遷移に伴う中性子スペクトルの解析を、終状態における相互作用模型をDWBA形式に拡張したモデルを用いて、中性子、重陽子とアルファ粒子への3体崩壊において、重陽子とアルファ粒子の相互作用が支配的であるという仮定の基に行った。この仮定及び模型は、Q-値範囲で－9 MeVまでの低励起状態に対応する遷移の中性子スペクトル及び角度分布を良く記述できることが判明した。一方、入射中性子と^{6}Li内のアルファ粒子の準弾性散乱に対応するQ-値領域では計算値とデータの一致は良好でなく、準弾性散乱の寄与が無視できない可能性が示唆された。

東海研究所：〒319－1195　茨城県那珂郡東海村白方白根2－4
+　先端基礎研究センター
*　東北大学
**　科学技術庁
*3　オランダエネルギー研究所
*4　ロスアラモス国立研究所

Contents

1. Introduction 1
2. Experimental Procedure and Data Reduction 2
2.1 Experiments 2
2.2 Data Reduction 3
3. Experimental Results 4
4. Theoretical Interpretations 5
4.1 Optical and DWBA Model Analysis 5
4.2 Analysis of the Continuum Spectra by Watson Theory of Final-state Interaction 6
4.2.1 Essensce of the FSI Theory 7
4.2.2 Pong-Austern Method 8
4.2.3 Werntz Method 9
4.2.4 Cross Section Formula 9
4.2.5 Gaussian Broadening 11
4.2.6 The d- α Phase-shift 11
4.2.7 Comparison with the Data 12
5. Discussion 12
6. Summary 14
Acknowledgements 14
References 15

目　　次

1. 序　論 …… 1
2. 実験及びデータ処理 …… 2
2.1 実験手法 …… 2
2.2 データ処理 …… 3
3. 実験結果 …… 4
4. 理論計算 …… 5
4.1 光型模型及びＤＷＢＡ …… 5
4.2 Watsonの終状態相互作用模型 …… 6
4.2.1 終状態相互作用模型の概略 …… 7
4.2.2 Pong-Austernの方法 …… 8
4.2.3 Werntzの方法 …… 9
4.2.4 断面積の公式 …… 9
4.2.5 ガウス関数による揺らぎ …… 11
4.2.6 重陽子-アルファ粒子間の位相差 …… 11
4.2.7 実験値との比較 …… 12
5. 議　論 …… 12
6. 結　論 …… 14
謝　辞 …… 14
参考文献 …… 15

1 Introduction

The ^{6}Li nucleus is known to have a predominant cluster structure, with the d-α probability in the ground state of around 0.70[1, 2, 3, 4]. Furthermore, the d-α breakup threshold is very low (1.475 MeV) due to the $2S$ weak-binding nature between these 2 particles. Because of those features, the breakup of ^{6}Li into d and α is one of the major reaction channels involving this nucleus from very low to high energies. Consequently, the structure and breakup reaction of ^{6}Li have been a subject of long and intensive studies as described in, e.g., Refs. [2, 3, 4, 5, 6, 7, 8, 9, 10, 11, 12, 13, 14, 15] and references therein.

The breakup of ^{6}Li nucleus into d + α at low relative energy region is also of a big interest from the astrophysics point of view, because the radiative capture reaction d + $\alpha \rightarrow$ ^{6}Li + γ at very low energies ($E_{cm} \leq$ 10-100 keV) is one of the key reactions in the nucleosynthesis in the early Universe or during stellar evolution[16]. Baur et al.[17] has suggested to use the Coulomb-breakup of ^{6}Li projectile to study the ^{6}Li + $\gamma \rightarrow$ d + α process by absorption of a virtual photon, which is the time-reversed process of the radiative capture. A couple of experiments have been already carried out to extract the astrophysical S factor according to this concept[18]. They have argued that the nuclear breakup contribution is negligible at extremely forward angles. However, it was pointed out by Hirabayashi and Sakuragi[19] that the nuclear contribution is as important as the Coulomb breakup even at very forward angles. Therefore, an accurate treatment of the nuclear breakup of ^{6}Li is essential to interpret the data from such experiments. In this sense, the neutron - ^{6}Li reaction provides a unique testing ground for theories since only the nuclear breakup is present there.

The few-body, especially three-body, problem is still an open (and therefore interesting) subject in nuclear physics, and has been studied intensively by various theoretical frameworks[20, 21, 22, 23, 24, 25]. At low-bombarding energies, such a multi-particle decay is known to proceed as a sequential reaction via intermediate states, which are definite states of particle-unstable systems[26, 27, 28, 29]. For example, a reaction sequence like

$$n + {}^6\mathrm{Li} \rightarrow n' + {}^6\mathrm{Li}^* \quad ,$$
$$ {}^6\mathrm{Li}^* \rightarrow d + \alpha,$$

will be the dominant one for n + ^{6}Li reaction, while other intermediate states such as ^{5}He* or t are also possible. In this mechanism, the Final-State Interaction (FSI) effect, in other words the interaction between, e.g., d and α, is particularly important to comprehend the particle spectra at the final states. In the Watson theory[20], the effect of the FSI is factored out from the T-matrix element so that the wave function of the 2 particles interacting in the final-state determines the essential cross section dependence on the secondary particle energy. This method, which we will use in the present work, has been applied to analyze breakup reactions of light nuclei at low projectile-energy region because of its simplicity, and has been able to extract the basic reaction mechanisms dominating a certain reaction channel[26, 27, 28, 29, 30, 31, 32, 33, 34, 35].

Beside these basic interests, the neutron interaction with ^{6}Li is important from the application point

of view, since lithium is the major tritium breeding material in thermonuclear fusion reactor system. The data for (n,n')dα reaction is particularly important because the statistical model, which is used often in evaluation of nuclear data for medium to heavy nuclei, cannot be applied to the few-body breakup process of light nuclei[36, 37].

In spite of the importance of the n + ^{6}Li reaction as described above, the ^{6}Li(n,n') reaction data leading to continuum breakup process is extremely rare. Except for several data at 14 MeV or below[38, 39, 40], there is only one data point at 18 MeV[41]. In Ref. [41], they have measured the (n,n') spectra at 18 MeV, and have shown that the FSI formula given by Werntz et al.[30], with the assumption of d-α FSI, can explain the major part of the neutron spectra at low d-α relative energy domain by taking account of the S- and D-waves in d-α system. That work, however, suffered from several deficiencies. Firstly, the experimental resolution was not good enough, so there was a considerable "tail" of the elastic scattering in the continuum spectra. Secondly, there was an appreciable background coming from the D(d,np)d neutrons produced from the neutron source, elastic scattering of which coincides with the (n,n') continuum part. Because of these reasons, their data could not be considered to be very reliable. Furthermore, they have used in the FSI theory analysis the d-α phase-shift data read from an article graphically, which may not be necessarily very accurate.

The purpose of this work is to carry out a series of neutron-induced neutron-producing data measurement on ^{6}Li at 11 to 18 MeV region with improved energy resolution compared with our previous works[40, 41] to enhance the database on this nucleus. Then, an optical model potential, which can describe the neutron elastic and total cross sections of ^{6}Li in a broad energy range, is developed, and is utilized in the analysis of the inelastic data via the macroscopic-vibrational DWBA formalism. Secondly, the measured data are employed to test the Watson FSI theory extended to DWBA form by Pong-Austern[33] and Datta et al.[35], which will be of particular importance for nuclear data evaluation purposes[36, 37] due to its simplicity in practical computation.

In the following sections we discuss the experimental details, development of the optical model and DWBA analysis of inelastic scattering data, and FSI theory analysis of the (n,n') continuum spectra.

2 Experimental Procedure and Data Reduction

2.1 Experiments

Experiments were carried out for 14.1 MeV, 18.0 MeV and 11.5 MeV incident neutrons using the Tohoku University Dynamitron time-of-flight(TOF) spectrometer. The details of the experimental procedure are described in refs[42, 43, 44, 45]. In the 14.1 MeV and 18 MeV measurements, we achieved an improved energy resolution than that in previous works[40, 41] as described below. The data for 11.5 MeV neutrons were obtained by using the ^{15}N(d,n) source and a "double-time-of-flight method" (inverse scattering geometry) to eliminate background events due to non-monoenergetic components in the source.

Source neutrons were produced via the T(d,n) reaction for 14.1 MeV and 18 MeV measurements and

the ^{15}N(d,n) reaction for 11.5 MeV measurement by bombarding a tritium loaded titanium target and a ^{15}N gas target, respectively, with a deuteron beam. For 18 MeV neutron production, we used a target thinner than in previous works[41] to improve the energy resolution. Pulsed deuteron beam with a 1.5 to 2.0 ns duration (FWHM) and a 2.0 MHz repetition rate was provided by a 4.5 MV Dynamitron accelerator with a post acceleration chopping system (PACS)[46]. PACS reduces the beam pulse "tail" remarkably so that we obtained clear separation among neutrons from the discrete levels. Scattering sample was a cylinder of enriched metallic ^{6}Li (95% in ^{6}Li), 3.2-cm-diam × 4-cm-long and placed 12 cm from the neutron target. The secondary neutron detector was a cylindrical NE213 scintillation detector, 14-cm-diam × 10-cm-long for 14.1 MeV neutrons and a long liquid scintillation detector (LLSD) of NE213 [47, 48], 80-cm-long × 10-cm-wide × 6.5-cm-thick for 11.5 MeV and 18 MeV neutrons. LLSD has a counting efficiency about three times as large as that of 14-cm-diam × 10-cm-long and compensated the lower intensity of primary neutrons than in 14.1 MeV. The flight path was around 5 m for 11.5 MeV, and 6 m for 14.1 MeV and 18 MeV measurements.

The source neutron spectra for 18 MeV, 14.1 MeV and 11.5 MeV measurements are shown in Fig. 1. Neutrons were obtained at 0 degree emission angle except for the 14.1 MeV case where neutrons to 97.5 degree were used in order to reduce the energy spread. The energy spread of primary neutrons were around 400 keV for 18 MeV and 11.5 MeV, 150 keV for 14.1 MeV measurement in FWHM. In addition to the primary neutrons, lower energy neutrons are existing with significant intensity in each spectrum. The 14.1 MeV and 18 MeV source spectra were contaminated with neutrons by parasitic reactions (D(d,n)) and C(d,n) etc) and target scattering. The sample-dependent backgrounds due to these neutrons distorted the TOF spectra seriously and were removed by Monte Carlo calculations[49] for 14.1 MeV and 18 MeV data. On the other hands, the 11.5 MeV neutron source by the ^{15}N(d,n)^{16}O reaction is not monoenergetic but accompanied by intense background neutrons below 6 MeV corresponding to the several excited states of residual ^{16}O and their effects are too large to correct for by the calculation. We employed, therefore, the "double-time-of-flight (D-TOF) method"[44] to remove their effects experimentally. In D-TOF, the target-sample distance was extended to $\sim$ 3.2m and secondary neutrons were detected by the NE213 detector, 14-cm-diam × 10-cm-long and 12-cm-diam × 5-cm-long, at 80cm flight path. More details are described in ref[44, 43].

The TOF spectra were measured at 12 or 13 scattering angles between 20 and 150 degree at 14.1 and 18.0 MeV. On the other hand, the TOF spectra were measured at 11.5 MeV for the continuum part at 60 and 120 degrees only, while the elastic scattering and inelastic scattering to the first excited state was measured at 13 angles from 20 to 150 degrees.

2.2 Data Reduction

The TOF spectra were converted into energy spectra considering the effects of sample-independent background and the detection efficiency. The detection efficiency was deduced from the measurements of the ^{252}Cf spontaneous fission spectrum for low energy region (below about 4 MeV) and the calculations with the SCINFUL code[50] for high energy part (above about 4 MeV). Absolute cross sections were

determined relative to the ^{1}H(n,n) cross section by measuring a scattering yield from a polyethylene sample. The energy spectra were corrected for the finite sample-size effect by a Monte Carlo code SYNTHIA[49]. For 14.1 MeV and 18 MeV data, the effects of the parasitic neutrons were also removed concurrently by this code. In the Monte Carlo calculation, we used the JENDL-3.2 data as input data for neutron interaction with the ^{6}Li. The calculation results reproduced the experimental data generally well over the energy and angle and therefore provided reasonable correction factors. The angular-differential cross sections of the elastic and inelastic (E_x = 2.19 MeV) scattering were deduced from the double-differential cross sections by integrating them over the peak region.

3 Experimental Results

Examples of the measured double-differential cross sections are shown in Fig. 2 for pairs of incident energy and emission angle of (11.5 MeV, 60-deg.), (14.1 MeV, 30-deg.) and (18.0 MeV, 30-deg.). Arrows show the positions of secondary neutron energies for elastic (E_x =0) and inelastic scattering corresponding to the excited states of ^{6}Li at E_x = 2.186 MeV (3^+), 3.563 MeV (0^+, T=1), 4.31 MeV (2^+), 5.37 MeV (2^+, T=1) and 5.64 MeV (1^+). It must be noted that these excited states, except for those with T=1, are all particle unbound, and they break up mostly to d and α. In other words, they are the resonant states of these 2 particles.

The solid curves in Fig. 2 represent the 3-body phase-space distribution, which is valid if there is no interaction between n, d and α in the final state, and is given by[51]

$$\rho_3^{lab}(E_{n'}^{lab},\theta_{n'}^{lab}) = \frac{2}{h^6}\frac{\sqrt{M}(m_n m_d m_\alpha)^{3/2}}{(m_d+m_\alpha)^2}\sqrt{E_{n'}^{lab}\left(\frac{m_d+m_\alpha}{M}E_{tot}^{cm} - E_{n'}^{lab} + 2a_1\sqrt{E_{n'}^{lab}}cos\theta_{n'}^{lab} - a_1^2\right)} \quad (1)$$

where

$$a_1 = \frac{\sqrt{m_n m_p E_p^{lab}}}{m_p+m_T}, \quad (2)$$

$$E_{tot}^{cm} = Q + \frac{m_T E_p^{lab}}{m_p+m_T}, \quad (3)$$

$$M = m_n + m_d + m_\alpha, \quad (4)$$

and m denotes the mass of a particle represented by the subscript (p =projectile, T=target). On the other hand, the broken curves show the neutron spectra from the process

$$^6\mathrm{Li} + n \rightarrow d + {}^5\mathrm{He}\ ,$$
$$^5\mathrm{He} \rightarrow n' + \alpha$$

which was calculated by Beynon's kinematics formula[34]. The phase-space factor and Beynon's function are normalized to the data at each energy/angle point.

Figure 2 shows that there is a noticeable deviation from the phase-space distribution at the excitation energy region up to 6 MeV or higher, which corresponds to the known excited ^{6}Li states, showing a clear evidence of the d-α final state interaction. However, those states with T=1 will not be contributing

significantly, because the 3.563 MeV state does not enhance the spectra. The process leading to the intermediate ^{5}He nucleus results in neutron energies much smaller than the d-α FSI domain.

There is a possibility that the n-α quasi-free scattering (QFS) contributes to the spectra at the d-α FSI region, because the neutron energy corresponding to QFS coincides with the excitation of about 4.3 MeV, as indicated in the same figure. Here, the n-α QFS (q=0) denotes the elastic scattering of neutrons with α particle in the ^{6}Li target with 0 relative d-α momentum, after the binding energy is corrected, and treating the deuterium as the spectator. However, it is known that such QFS process leads to a rather flat particle distribution[12], so it will not produce an appreciable structure as seen in the present data at this energy region. We will return to this point later.

Other process, such as (n,2n) reaction, is known to produce very soft neutron spectra[40]. The bump toward the lower energy below 4 MeV at the projectile energy of 14.1 and 18.0 MeV will probably be due to such a process, which is again well separated from the d-α FSI region.

Therefore, we can conclude that the d-α FSI is the dominant reaction mechanism at low relative energy region in the residual d-α system which causes the neutron spectra to deviate significantly from the phase-space distribution.

4 Theoretical Interpretations

4.1 Optical and DWBA Model Analysis

A spherical optical model analysis was carried out by taking account of the total cross section data and elastic scattering angular distribution data simultaneously. We have included our elastic scattering data at 11.5, 14.1 and 18.0 MeV. Other data were retrieved from EXFOR system at NEA Data Bank, and a grid search procedure based on Metropolice method was performed to seek for the minimum chi-square. The results were then put to ECISVIEW system by Koning[52] and the parameters were slightly adjusted to get a better result. This result was further fed into a search procedure based on the Bayesian method[53] to get the final parameter set.

We have adopted a following form of the potential:

$$\begin{aligned} U = & - (V_r + iW_v) f(r, r_v, a_v) + 4ia_d W_d \frac{d}{dr} f(r, r_d, a_d) \\ & + \left(\frac{\hbar}{m_\pi c}\right)^2 \ell \cdot \mathbf{s}\, V_{so} \frac{1}{r} \frac{d}{dr} f(r, r_{so}, a_{so}), \end{aligned} \tag{5}$$

where the form factors f are of the standard Woods-Saxon shape

$$f(r, r_x, a_x) \equiv \frac{1}{1 + \exp\left((r - r_x A^{1/3})/a_x\right)}. \tag{6}$$

Here, the a_x is the diffuseness parameter, and A the target mass number. The potential depths were assumed to have the energy dependence similar to the one used by Delaroche et al.[54]:

$$V_r = V_0 e^{-\lambda_v (E - E_F)} + V_1 \tag{7}$$

$$W_d = W_{d_0} e^{-\lambda_{W_d}(E-E_F)} \frac{(E-E_F)^4}{(E-E_F)^4 + W_{d_1}^4} \tag{8}$$

$$W_v = W_{v_0} \frac{(E-E_F)^4}{(E-E_F)^4 + W_{v_1}^4} \tag{9}$$

$$V_{so} = V_{so} e^{-\lambda_{so}(E-E_F)} \tag{10}$$

The symbol E_F denotes the Fermi energy, and was calculated as

$$E_F = -\frac{1}{2}\left(S_n(A) + S_n(A+n)\right) \tag{11}$$

where $S_n(A)$, $S_n(A+n)$ denote the neutron separation energy from the target nucleus (A) and target + n nucleus (A+n), respectively. The calculation was done with ECIS96 optical model code with the relativistic kinematics option turned on.

We have found 2 sets of potentials that equally describe the experimental data. Those parameters are given in Table 1 as Set-1 and Set-2. The results of the present analysis are shown in Figs. 3 (total cross section) and 4 (elastic scattering).

The inelastic scattering cross section to the first excited 3^+ state was calculated by the DWBA formalism, assuming the collective-vibrational model, and by using the present optical potentials. The result is given in Fig. 5.

It is interesting that the 2 OMPs, which give the same description for the elastic scattering and total cross sections, give noticeably different predictions of the inelastic angular distribution at backward angles. At low energy (11.5 MeV), Set-2 seems to describe the data better, but the opposite tendency is true at 14.1 and 18.0 MeV.

The normalization constants for the DWBA cross section to reproduce the measured excitation of 2.186-MeV level was found to be 0.95 for Set-1, and 1.15 for Set-2 OMPs. These values are too large to be interpreted as the square of the deformation parameters in the normal vibrational model. Instead, it should be interpreted to be more of a nature of the proportionality factor for the effective nucleon-nucleon interaction in n+^{6}Li reactions. Indeed, the fact that the normalization constants obtained in the present analysis are close to unity shows that the effective nucleon-nucleon strength is almost similar for the diagonal part (OMP) and the off-diagonal part (transition form factor) of the interaction potential, as is the case for the coupled-discretized continuum channels (CDCC) formalism, where a common N_R and N_I parameters are multiplied to both the diagonal and off-diagonal potentials constructed from the M3Y interaction[10].

4.2 Analysis of the Continuum Spectra by Watson Theory of Final-State Interaction

It was shown in the previous sections that the final-state interaction (FSI) between deuteron and α particles, originally confined in the target ^{6}Li nucleus, plays an essential role in producing the continuum part of the neutron spectra at relatively high neutron energy, corresponding to the excitation energy below several MeV. Therefore, the FSI effect, together with the 3-body kinematics have to be

considered for a quantitative understanding of this part of the continuum neutron spectra produced via the ^{6}Li(n,n'd)α reaction. Here, we follow the basic framework established by Watson[20], which was extended by Pong-Austern[33] and Datta et al.[35] to the DWBA form. For completeness purpose, we give firstly the essence of the theory that we will utilize for the analysis.

4.2.1 Essensce of the FSI theory

The total Hamiltonian (H) for the three-particle system is assumed as $H = H_0 + U + V$, where H_0 is the free Hamiltonian for 3 particles, U the potential acting between the two particles (d and α in our case) at the final-state, and V the residual interaction. The transition matrix element T_{ba} between the initial channel a (^{6}Li + n) and the final channel b (n + d + α) is therefore given by

$$T_{ba} = \langle \chi_b^- | (U+V) | \psi_a^+ \rangle \tag{12}$$

where $\psi^\pm$ and $\chi^\pm$ denotes the complete three-particle wave function and free three-particle wave function, respectively, with the appropriate boundary condition corresponding to the subscript $\pm$.

The Lippman-Schwinger equation for ψ is given by

$$\psi^\pm = \chi^\pm + (E - H_0 \pm i\epsilon)^{-1}(U+V)\psi^\pm \tag{13}$$

Here, E is the total energy of the system. In the Watson theory, the transition matrix element Eq. (12) is modified in the following way so that the FSI effect is easily factored out from the T-matrix element.

The exit channel three-particle wave-function ϕ is defined in a way that a pair of d and α interacts via potential U while the neutron stays free,

$$\phi^\pm = \chi^\pm + (E - H_0 \pm i\epsilon)^{-1} U \phi^\pm \tag{14}$$

On the other hand, the entrance channel wave function ψ_0 consists of 3 particles (^{6}Li = d + α bound state and neutron in our case) interacting via the effective potential V alone, i.e., U=0;

$$\psi_0^\pm = \chi^\pm + (E - H_0 \pm i\epsilon)^{-1} V \psi_0^\pm \tag{15}$$

The T-matrix element of Eq. (12), together with Eqs. (13) and (14) yields

$$T_{ba} = \langle \psi_b^- | V | \psi_a^+ \rangle + \langle \chi_b^- | U | \phi_a^+ \rangle \tag{16}$$

It is Watson's argument that the FSI potential U is chosen so that the second term of this expression vanishes. The first term is then further modified, by utilizing Eq. (15), as

$$T_{ba} = \langle \phi_b^- | V | \psi_{0_a}^+ \rangle + \langle \psi_b^- - \phi_b^- | U | \psi_{0_a}^+ \rangle . \tag{17}$$

Now, the residual interaction V is assumed to be weak, so ψ_b tends to ϕ_b, and consequently the second term in the last equation can be omitted. The final form of the T-matrix element is thus written

$$T_{ba} = \langle \phi_b^- | V | \psi_{0_a}^+ \rangle . \tag{18}$$

In this expression, the effect of the final-state interaction U is contained only in ϕ_b.

The exit channel wave function ϕ_b can be separated into two parts, ignoring the spin-function of neutron;

$$\phi_b = \phi_{d\alpha}(\mathbf{k}_{d\alpha}, \mathbf{r}_{d\alpha}) X(\mathbf{k}_n, \mathbf{R}_n) \tag{19}$$

where $\phi_{d\alpha}(\mathbf{k}_{d\alpha})$ is the unbound wave function for the d-α system, $X(\mathbf{k}_n, \mathbf{R}_n)$ is a wave function for the relative motion between neutron and center-of-mass of the d-α system. By employing the usual DWBA approximation for the transition matrix, we get for T_{ba} an expression

$$T_{ba} = \langle \phi^-_{d\alpha} X^- |V| \; R^+ \phi_{^6Li} \rangle \tag{20}$$

where R^+ is the relative wave function between the projectile and ^{6}Li in the entrance channel, and $\phi_{^6Li}$ is the intrinsic wave function of the target ^{6}Li nucleus.

According to Pong and Austern, we now make a following approximation to factor out the dependence of the T-matrix on the final-state particle energy with an assumption of the short-range nature of the residual interaction V:

$$V\phi_{d\alpha}(\mathbf{k}_{d\alpha}) \sim A(E) V W(\mathbf{k}_{d\alpha}, \mathbf{r}) \tag{21}$$

where $A(E)$ carries the bulk of the energy dependence, $E = \hbar^2 k^2_{d\alpha}/(2\mu_{d\alpha})$, and $W(\mathbf{r}, \mathbf{k}_{d\alpha})$ is a relatively energy independent d-α bound wave function, having a specific spin structure and normalized to unity within a certain radius $r = R_0$. With this form inserted in Eq. (20), we obtain

$$\begin{aligned} T_{ba} &= A(E) \langle W^-_{d\alpha} X^- |V| \; R^+ \phi_{^6Li} \rangle \\ &= A(E) T^{DW}_{ba} \end{aligned} \tag{22}$$

where T^{DW}_{ba} denotes the normal DWBA T-matrix with bound-state final-state wave function.

The enhancement factor $|A(E)|^2$ is calculated by utilizing the relation

$$\begin{aligned} |A(E)|^2 &= |A(E)|^2 \int_0^{R_0} r^2 dr \int d\Omega \, |W(\mathbf{k}_{d\alpha}, \mathbf{r})|^2 \\ &= \int_0^{R_0} r^2 dr \int d\Omega \, |\phi^-_{d\alpha}(\mathbf{k}_{d\alpha}, \mathbf{r})|^2 \end{aligned} \tag{23}$$

where $d\Omega$ denotes an integral with respect to angles and any internal coordinates (such as spin). Writing $\phi^-_{d\alpha}(\mathbf{r}, \mathbf{k}_{d\alpha}) = [\chi(\mathrm{k,r})/\mathrm{r}]Y$ where Y represents a proper (normalized) spin-angle wave function, we get

$$|A(E)|^2 = \int_0^{R_0} dr \, |\chi(k, r)|^2 \tag{24}$$

Now, we adopt 2 methods to evaluate the right-hand side of this equation.

4.2.2 Pong-Austern method

Pong and Austern had transformed the integral in the r.h.s. of the above equation to a surface limit using the radial Schrödinger equation. Furthermore, by assuming that the energy derivative of the

Coulomb function is small compared with the derivative of the nuclear phase shift δ, they have arrived at the following formula:

$$|A(E)|_c^2 \sim \frac{d\delta_c}{dE} \tag{25}$$

where subscript c specifies the partial wave state, i.e., c represents ${}^{2S+1}L_J$ in the usual notation.

4.2.3 Werntz method

If we take an assumption that the residual interaction V is of the surface-peaked δ-function form, only the wave function value at the nuclear surface (a) is relevant. Therefore, the Eq. (24) can be written in this case to be

$$|A(E)|_c^2 \sim |\chi(k,a)_c|^2 \tag{26}$$

The wave function value at the surface $\chi(k,a)$ may be evaluated by using the external solution

$$\chi(k,r)_c = (k)^{-1}[\cos(\beta_c)F_L(kr) + \sin(\beta_c)G_L(kr)] \tag{27}$$

where β_c is nuclear phase-shift for elastic d-α scattering, and G_L and F_L being the Coulomb wave-functions which are irregular and regular at the origin. Then, we arrive at the following expression:

$$|A(E)|_c^2 \sim \sin^2(\delta_c)\frac{G_L^2(ka) + F_L^2(ka)}{k^2} \tag{28}$$

where $\delta_c = \alpha_c + \beta_c$, and $\alpha_c = \tan^{-1}[F_L(ka)/G_L(ka)]$.

The two expressions (Eqs. (25) and (28)) give essentially the same energy dependence for the enhancement factor around an isolated resonance. For example, if we assume a resonance of the form

$$\delta(E_c) = \tan^{-1}\left(\frac{\frac{1}{2}\Gamma_c}{E - E_{0_c}}\right) \tag{29}$$

where Γ_c and E_{0_c} denotes the resonance width and resonance energy for partial wave c respectively, Eq. (25) leads to the following Breit-Wigner type enhancement factor:

$$|A(E)|_c^2 = \frac{\frac{1}{2}\Gamma_c}{(E - E_{0_c})^2 + \left(\frac{1}{2}\Gamma_c\right)^2} \tag{30}$$

This shape is also reproduced by the $\sin^2(\delta)$ part in Eq. (28) very well. The main difference between these 2 formulae comes from the presence of the second factor in Eq. (28), which may not be significant around sharp resonances (this corresponds to taking the Γ_c constant). Phillips et al.[22] has also derived essentially the same expressions from discussion on the generalized density of states functions. In this work, we will use the formula Eq. (28) because the Coulomb function present in Werntz formula will be important due to the broadness of resonances in the d-α system.

4.2.4 Cross Section Formula

The double-differential cross section σ_c for a specific final partial-wave state c is related to the transition amplitude by

$$\sigma_c \equiv \frac{d^2\sigma_c}{dE_n d\Omega_n} = \frac{2\pi}{\hbar v}|T_{ba}|_c^2 \rho_n \rho_{d\alpha} \tag{31}$$

where ρ_n and the $\rho_{d\alpha}$ are the phase-space density for the residual n + ^{6}Li* system and d + α system, respectively, and v is the projectile velocity. It is known that these 2-body phase-space density is proportional to the velocity (or the wave number) of the relative motion in each pair. Therefore they could be expressed as

$$\rho_n = \frac{\mu_{n^6Li^*}\hbar k_{n^6Li^*}}{(2\pi\hbar)^3}, \tag{32}$$

$$\rho_{d\alpha} = \frac{\mu_{d\alpha}\hbar k_{d\alpha}}{(2\pi\hbar)^3} \tag{33}$$

with the obvious condition coming from energy conservation

$$\frac{(\hbar k_{n^6Li^*})^2}{2\mu_{n^6Li^*}} + \frac{(\hbar k_{d\alpha})^2}{2\mu_{d\alpha}} = E_{tot}^{cm} \tag{34}$$

where E_{tot} is the total available energy in the cm system, μ denotes the reduced mass in the system specified by the subscript. With the condition of Eq. (34), the product of 2 phase-space volumes in Eq. (31), $\rho_n\rho_{d\alpha}$ combines to produce the 3-body phase-space factor ρ_3[51]. By putting Eq. (22) into Eq. (31), the cross section is now written as

$$\sigma_c = \frac{2\pi}{\hbar v}|A(E)|_c^2|T_{ba}^{DW}|_c^2\rho_3 \tag{35}$$

$$= |A(E)|_c^2\sigma_c^{DW}\rho_{d\alpha} \tag{36}$$

where

$$\sigma_c^{DW} = \frac{2\pi}{\hbar v}|T_{ba}^{DW}|_c^2\rho_n \tag{37}$$

is the cross section calculated by the DWBA formalism assuming ^{6}Li* to be a bound system of d and α in partial wave state c.

We assume that this formula holds for each partial wave state c independently, so the total cross section is an incoherent sum of the contributions from various partial-wave states:

$$\sigma^{cm} = \sum_c N_c\sigma_c \tag{38}$$

where N_c is the normalization constant for each partial wave state c to take account of the possible difference in the transition strength to each channel $c \equiv {}^{2S+1}L_J$. This expression is then converted to the laboratory frame to compare with the experimental data:

$$\sigma^{lab} = J\sigma^{cm} \tag{39}$$

The Jacobian of transformation J is given by[51]

$$J \equiv \frac{\partial(E_n^{cm}, cos\theta_n^{cm})}{\partial(E_n^{lab}, cos\theta_n^{lab})} = \sqrt{\frac{E_n^{lab}}{E_n^{cm}}} \tag{40}$$

If we take a rather radical assumption that the T-matrix element in Eq. (35) is constant, the partial-wave cross section becomes of the form

$$\sigma_c^{lab} \sim |A(E)|_c^2\rho_3^{lab} \tag{41}$$

where $\rho_3^{lab} \sim J\rho_3$. This is the form employed in many works with Werntz enhancement formula [31, 32], including our previous one[41]. In the present work, however, we will adopt the form of Eqs. (36) and (37).

4.2.5 Gaussian broadening

The calculated cross section must be broadened by considering the finite resolution of the experimental apparatus to be compared with the measured data. We assume that the energy resolution function G is expressed by a Gaussian form,

$$G(E, E', w) = \frac{1}{\sqrt{2\pi}w} e^{-\frac{(E-E')^2}{2w^2}}, \tag{42}$$

where the standard deviation w consists of 2 components

$$w = \frac{1}{2\sqrt{2}\ln(2)} \sqrt{w_E^2 + w_T^2}. \tag{43}$$

Here, the first term (w_E) denotes the contribution from the finite energy resolution (in FWHM) of the neutron source due mostly to the energy reduction of the deuterium beam in the neutron producing target, while the second term (w_T) represents the energy spread caused by the finite timing resolution expressed in FWHM. The latter term is written more explicitly by using the time-of-flight resolving power $R = \Delta_T/L$, where Δ_T denotes the timing resolution and L the flight path,

$$w_T = \frac{2}{72.3} E^{3/2} R. \tag{44}$$

In the above expression, energy E is expressed in [MeV], Δ_T in [ns], and L in [m].

The double-differential cross section, $\sigma(E, \Omega)^{broad}$, which includes the resolution broadening and can be compared with the experiment, at secondary energy E and angle Ω, is then calculated as

$$\sigma(E, \Omega)^{broad} = \int dE' G(E, E', gw(E'))\sigma(E', \Omega) \tag{45}$$

where the Gaussian width w, Eq. (43), is calculated at energy E'. In actually applying this formula, the Gaussian width w was multiplied by an adjustable parameter g to account for other sources, such as angular resolution, which contribute to broaden further the spectra. The parameter g was determined to reproduce the width of the observed elastic scattering peak.

4.2.6 The d-α Phase-Shift

The d-α phase shift data, δ_c, were obtained from the R-matrix analysis of the ^{6}Li system by G. Hale et al.[55] up to deuteron energy of 7 MeV. Over 1000 data points, including the elastic d-α scattering and deuteron analyzing power data, have been included in this analysis. The results of the R-matrix analysis was found to be essentially good even for higher energy except for the partial waves of $^3S_1$, $^3D_1$ and $^3D_3$. Therefore, the phase-shifts for these partial waves were slightly modified to match the data above relative d-α energy of 7 MeV. The results are shown in Fig. 6. Here, the partial waves $^3S_1$, $^3D_1$, $^3D_2$ and $^3D_3$ show remarkable resonant behaviors, i.e., crossing of $\delta = 90$ degree, corresponding to the excited states in ^{6}Li, while $^3P_0$, $^3P_1$, $^3P_2$, $^3F_2$, $^3F_3$, $^3F_4$, $^3G_3$, $^3G_4$ and $^3G_5$ partial waves have more off-resonant behaviors. The main structure in the secondary neutron spectra, therefore, is expected to come from the contributions from the former 4 partial waves, while the rests will form more or less "background" components. The channel radius for d-α system was chosen to be 4.62 fm.

4.2.7 Comparison with the Data

We have included the following 5 partial waves, $^3S_1$, $^3P_0$, $^3D_1$, $^3D_2$, and $^3D_3$ in the FSI formula given previously. Contributions from the other states were replaced by the 3-body phase space factor ρ_3^{lab} given the smooth nature of the phase-shifts for these partial waves. A delta-function was also inserted to represent the elastic scattering peak, which leads to a usual Gaussian function after Gaussian broadening. Therefore, the fitting formula becomes

$$\sigma = G\left[N_{ela}\delta(E - E_{ela}) + \sum_c N_c\sigma_c^{lab} + N_{ps}\rho_3^{lab}\right], \tag{46}$$

where $G[...]$ denotes the Gaussian broadening, $\delta(E - E_{ela})$ is for the elastic scattering peak located at $E = E_{ela}$, and $c = {}^3S_1$, $^3P_0$, $^3D_1$, $^3D_2$ and $^3D_3$.

The DWBA cross sections contained in the σ_c^{lab} were calculated with the macroscopic-vibrational model with optical potential Set-1, with the excitation energy interval of 0.5 MeV and angular interval of 1-degree, and for the orbital angular momentum transfer of 0, 1 and 2. Such 2-dimensional table was employed to interpolate the values needed at a specific excitation energy and angular point. The normalization coefficients, N_{ela}, N_c and N_{ps} were determined by the least-squares method. These normalization coefficients were firstly determined at each projectile energy and angle point, and then they were averaged over angles at each projectile energy. As a result, it turned out that the contribution from the $^3P_0$ and $^3D_1$ partial waves were almost negligible at all projectile energies, so we ignored these partial waves in the final analysis.

The effect of the Gaussian broadening is demonstrated in Fig. 7 for the partial waves of $^3S_1$, $^3D_2$, $^3D_3$, and the phase-space (PS) factor. The net effect of the broadening is significant for $^3D_3$, less significant but noticeable for the $^3D_2$ partial waves. For $^3S_1$ and PS, the effect is almost negligible.

The calculated values are compared with the measured data at selected angles in Fig. 8. In this figure, the experimental data are shown as open circles, the elastic scattering peak as the broken curves, the $^3S_1$ contribution by the dash-dotted curves, the $^3D_2$ by the thin solid curves with dot, $^3D_3$ by the thin solid curves, and the phase-space (PS) component by the long broken curves. The present calculation reproduces the general feature of the measured data very well, except for the very low secondary neutron energy region, where the contribution other than the d-α FSI, such as the (n,2n) or n-α FSI, will be dominant. It is obvious that, at all projectile energies, the $^3D_2$ and $^3D_3$ partial waves are the major channel in the neutron inelastic scattering, while the $^3S_1$ and PS contributes as the background.

5 Discussion

The 2 OMPs, Set-1 and Set-2 in Table 1, were found to be able to describe the elastic scattering and total cross section of ^{6}Li above 7 MeV very well. Indeed, a preliminary result of a measurement by Dietrich carried out at WNR indicates that the present OMPs can describe the total cross section of ^{6}Li up to 500 MeV[56]. The possibility of predicting the data up to such a high energy is an important feature in application fields.

The present potentials are characterized by large diffuseness parameters, i.e., a of about 0.7 (Set-1) or 0.8 (Set-2). This will probably be a reflection of the loose bound "$2S$" nature of the ^{6}Li ground state. The three-body calculations[1, 3] show that the s-wave d-α wave function has a node around 1.7 fm, and have a very long tail. The thickness of the surface predicted by these calculations is in good agreement with the diffuseness parameter obtained in the present work.

The root-mean square radius R_{OMP} are calculated from the presently-obtained real central OMP to be 3.2 fm (Set-1). This value yields the R_c (root-mean square radius for charge distribution) of 2.6 fm if the difference between the R_{OMP} and R_c is corrected based on the improved local-density approximation of jeukenn-Lejeune-Mahaux prescription[58, 59] with the matter and charge distributions calculated by the Hartree-Fock theory[60]. The value of R_c = 2.6 fm is in good agreement with the measured one of 2.56 ± 0.05 fm[3]. Therefore, the form factor of the optical potential obtained in the preset work is consistent with the major properties of the ground state of ^{6}Li.

The inelastic scattering to the first excited 3^+ state was also reproduced well by the DWBA calculation based on the macroscopic-vibrational model employing the present potentials. The normalization factor was found to be almost unity, which is consistent with the CDCC method if it is interpreted as the proportionality factor of the effective nucleon-nucleon interaction. However, it was shown by Hirabayashi and Sakuragi[19] that the use of a simple collective-vibrational form factor, i.e., derivative Woods-Saxon shape, is not consistent with the full-microscopic form factor derived by the CDCC theory[24]. The form factor calculated by the CDCC theory is wider than the collective one by about a factor of 1.5, due to the unbound nature of the 3^+ state. On the other hand, the difference between these 2 form factors is not very significant except for the width. Indeed, the calculated results are similar in the angular dependent shape except for the overall magnitude, which may be adjusted to match by changing the normalization constant of the transition form factors. We have also made a comparison of the real part of the transition form factor, and it is shown in Fig. 9. Here, the CDCC form factor was calculated for neutron-^{6}Li interaction[57], and was normalized to the present one. Obviously, the present form factor coincides with the one derived by the microscopic theory both in the peak position and peak width very well. This is again due mainly to the large diffuseness parameter in our potential. The difference in the interior region is not important because most of the reaction takes place at the exterior region, where the 2 methods yields very similar results. It must be stressed that we did not force the OMP search to coincide with the CDCC form factor. Therefore, the fact that the ^{6}Li have a diffuse ground state and unbound excited states seem to be implicitly embedded in the large diffuseness parameter, which our search gave us automatically. Just a simple prescription of making the a parameter larger than the normal values would be then an effective way in calculating cross sections for other light nuclei which have similar features. Anyway, it was confirmed that use of the simple macroscopic-vibrational model in calculation of inelastic neutron scattering from ^{6}Li with a large diffuseness parameter is a good approximation of the microscopic approach such as the CDCC theory.

As shown in Fig. 8, the present assumption of the d-α FSI and the Watson's theory extended to DWBA form gives a fairly good description of the experimental double-differential cross sections for

the low-excitation energy regions at all projectile energies. To show how the present model describes the angular distribution of neutrons corresponding to various Q-values, we have plotted the angular distribution of inelastically scattered neutrons wht 1-MeV Q-value intervals in Fig. 10. They have been converted to the center-of-mass system assuming the 2-body kinematics. The present model gives a very good overall agreement with the measured data, except fot the Q-value bins from -3 MeV to -4 MeV, and from -4 MeV to -5 MeV. One possible explanation of this discrepancy is the neutrons from the inelastic scattering to the 3.563 MeV (T=1) state, which was not considered in our model but falls in these Q-value bins. However, we do not think it is likely, because the cross section of exciting this state is estimated to be about 1 to 2 mb at this energy region. Another possibility is the n-α quasi-free scattering. The differential elastic n-α scatteing cross section has a very large value of around 100 to 200 mb/sr at this projectile energy region, and is very forward peaked. Probably, the n-α QFS is the reason for the discrepancy between the present calculation and the data for Q=-3 to 5 MeV region at the forward angular range. Except for these Q-value bins, however, the present model describes the data up to Q=-8 MeV for 14.1 MeV incident neutrons, and to -9 MeV for 18.0 MeV neutrons, covering the major part of the low-excitation regions.

6 Summary

We could construct a phenomenological optical model potential which can describe the neutron total cross section, elastic scattering angular distribution of ^{6}Li from 5 MeV to several tens MeV. This potential was also found to describe the inelastic scattering to the 1st excited state very well via the DWBA formalism. Therefore, this OMP will be a valuable tool for the future analysis of neutron interaction with ^{6}Li, which will be important from both the fundamental and applied points of view.

The analysis for the continuum neutron spectra, based on the Watson's final-state interaction theory extended to the DWBA form, was found to be of modest success. Probably we miss the contribution from the n-α quasi-free scattering. Such a contribution may be calculated by the PWIA or DWIA in principle, and added to the present calculation. However, we dare not to try such a calculation in this work, because the ability of the DWIA calculation for the QFS process of ^{6}Li itself is still a matter of open question[12]. Nevertheless, the model proposed in this work was able to describe the major part of the continuum neutron spectra to the Q-value range as deep as -9 MeV.

Acknowledgements

The authors are grateful to Dr. Y. Sakuragi and Dr. M. Kamimura for offering the CDCC form factors.

References

[1] D.R. Lehman and Mamta Rajan, Phys. Rev. **C25**, 2743(1982).

[2] R.E. Warner, R.S. Wakeland, J-Q. Yang, D.L. Friesel, P. Schwandt, G. Caskey, A. Galonsky, B. Remington and A. Nadasen, Nucl. Phys. **A422**, 205(1984).

[3] V.I. Kukulin, V.M. Krasnopol'sky, V.T. Voronchev and P.B. Sazonov, Nucl. Phys. **A417**, 128(1984).

[4] R. Ent, H.P. Blok, J.F.A. Van Hienen, G.Van der Steenoven, J.F.J. Van den Brand, J.W.A. den Herder, E. Jans, P.H.M. Keizer, L. Lapikas, E.N.M. Quint, P.K.A. de Witt Huberts, B.L. Berman, W.J. Briscoe, C.T. Christou, D.R. Lehman, B.E. Norum, and A. Saha, Phys. Rev. Lett. **57**, 2367(1986).

[5] M. Lemere, Y.C. Tang and H. Kanada, Phys. Rev. **C25**, 2902(1982).

[6] J.W. Watson, H.G. Pugh, P.G. Roos, D.A. Goldberg, R.A.J. Riddle and D.I. Bonbright, NUcl. Phys. **A172**, 513(1971).

[7] J.M. Lambert, R.J. Kane, P.A. Treado, L.A. Beach, E.L. Petersen and R.B. Theus, Phys. Rev. **C4**, 2010(1971).

[8] A.K. Jain, J.Y. Grossiord, M. Chevallier, P. Gaillard, A.Guichard, M. Gusakow and J.R. Pizzi, Nucl. Phys. **A216**, 519(1973).

[9] P.G. Roos, D.A. Goldberg, N.S. Chant, R. Woody III and W. Reichart, Nucl. Phys. **A257**, 317(1976)

[10] Y. Sakuragi, M. Yahiro and M. Kamimura, Prog. Theor. Phys. **70**, 1047(1983).

[11] J.R. Hurd, J.S. Boswell, R.C. Minehart, Y. Tzeng, H.J. Ziock, K.O.H. Ziock, L.C. Liu and E.R. Siciliano, Nucl. Phys. **A475**, 743(1987).

[12] C. Samanta, S. Ghosh, M. Lahiri, S. Ray and S.R. Banerjee, Phys. Rev. **C45**, 1757(1992).

[13] C. Samanta, T. Sinha, S. Ghosh, S. Ray and S.R. Banerjee, Phys. Rev. **C50**, 1226(1994).

[14] K. Rusek, P.V. Green, P.L. Kerr and K.W. Kember, Phys. Rev. **C56**, 1895(1997).

[15] B.S. Pudliner, V.R. Pandharipande, J. Carlson, S.C. Pieper and R.B. Wiringa, Phys. Rev. **C56**, 1720(1997).

[16] W.A. Fowler, Rev. Mod. Phys. **56**, 149(1984).

[17] G. Baur, C.A. Bertulani and H. Rebel, Nucl. Phys. **A458**, 188(1986).

[18] J. Kiener, H.J. Gils, H. Rebel, S. Zagromski, G. Gsottschneider, N. Heide, H. Jelitto, J. Werntz and G. Baur, Phys. Rev. **C44**, 2195(1991).

[19] Y. Hirabayashi and Y. Sakuragi, Phys. Rev. Lett. **28**, 1892(1992).

[20] K.M. Watson, Phys. Rev. **88**, 1163(1952).

[21] A.B. Migdal, Sov. Phys.-JETP **1**, 2(1955).

[22] G.C. Phillips, T.G. Grify and L.C. Biedenharn, Nucl. Phys. **21**, 327(1960).

[23] N.S. Chant and P.G. Roos, Phys. Rev. **C15**, 57(1977)

[24] Y. Sakuragi, M. Yahiro and M. Kamimura, Prog. Theor. Phys. Suppl. **89**, 136(1986).

[25] K. Miyagawa, Y. Koike, T. Ueda, T. Sawada and S. Takagi, Prog. Theor. Phys. **74**, 1264(1985).

[26] A.W. Parker, J.S. Allen, R.L. Yerke, and V.G. Shotland, Phys. Rev. **174**, 1093(1968).

[27] C. Moazed and H.D. Holmgre, Phys. Rev. **166**, 977(1968).

[28] M.A. Waggoner, J.E. Etter, H.D. Holmgren and C. Moazed, Nucl. Phys. **88**, 81(1966).

[29] J.D. Bronson, W.D. Simpson, W.R. Jackson and G.C. Phillips, Nucl. Phys. **68**, 241(1964).

[30] C. Werntz, Phys. Rev. **128**, 1336(1962).

[31] R.E. Warner an R.W. Bercaw, Nucl. Phys. **A109**, 205(1968).

[32] T. Rausch, H. Zell, D. Wallenwein and W. Von Witsch, Nucl. Phys. **A222**, 429(1974).

[33] W.S. Pong and N. Austern, Nucl. Phys. **A221**, 221(1974).

[34] T.D. Beynon and A.J. Oastler, Ann. Nucl. Energy **6**, 537(1979).

[35] S.K. Datta, W.R. Falk, S.P. Kwan, R. Abegg and O.A. Abou-Zeid, Phys. Rev. **C21**, 1687(1980).

[36] S. Chiba, T. Fukahori, K. Shibata, B. Yu and K. Kosako, Fusion Engineering and Design, **37**, 175(1997).

[37] T. Fukahori, S. Chiba, N. Kishida, M. Kawai, Y. Oyama and A. Hasegawa, "Status of JENDL Intermediate Energy Nuclear Data", Proc. of Int. Conf. on Nuclear Data for Science and Technology, May 1997, Trieste, Italy, to be published.

[38] P. Lisowski, G.F. Auchampaugh, D.M. Drake, M. Drosg, G. Haouat, H.W. Hill and L. Nilsson, , LA-8342 (1980).

[39] A. Takahashi, "Double Differential Neutron Emission Cross Sections at 14 MeV Measured at OKTAVIAN", JAERI-M 86-029, p.99(1986).

[40] S. Chiba, M. Baba, H. Nakashima, M. Ono, N. Yabuta, S. Yukinori and N. Hirakawa, J. Nucl. Sci. Technol. **22**, 771(1985).

[41] S. Chiba, M. Baba, N. Yabuta, T. Kikuchi, M. Ishikawa, N. Hirakawa and K. Sugiyama, "Measurement of neutron-induced neutron-producing cross sections of ^{6}Li and ^{7}Li at 18.0 MeV, Proc. of Int. Conf. on Nuclear Data for Science and Technology (1988 Mito), p.253, Saikon Publishing, Tokyo (1988).

[42] M.Baba, S.Matsuyama, T.Ito, T.Ohkubo and N.Hirakawa, J. Nucl. Sci. Technol. **31**, 757(1994).

[43] M.Ibaraki, M.Baba, S.Matsuyama, T.Sanami, Than Win, T.Miura and N.Hirakawa, Proc. of Int. Conf. on Nuclear Data for Science and Technology (1997 Trieste), to be published

[44] M.Baba, S.Matsuyama, M.Ibaraki, D.Soda, T.Ohkubo, T.Sanami, Than Win, T.Miura and N.Hirakawa, *ibid*, to be published.

[45] M. Ibaraki et al, to be submited to J. Nucl. Sci. Technol.

[46] S.Matsuyama, M.Fujisawa, M.Baba, T.Iwasaki, S.Iwasaki, R.Sakamoto and K.Sugiyama, Nucl. Instr. Methods **A348**, 34(1994).

[47] S.Matsuyama, T.Ohkubo, M.Baba, S.Iwasaki, D.Soda, M.Ibaraki and N.Hirakawa, *ibid*, **A372**, 246(1996).

[48] S.Matsuyama, D.Soda, M.Baba, S.Iwasaki, M.Ibaraki, T.Ohkubo, Y.Nauchi and N.Hirakawa, *ibid*, **A384**, 439(1997).

[49] M.Baba, S.Matsuyama, M.Ishikawa, S.Chiba, T.Sakase and N.Hirakawa, *ibid*, **A366**, 354(1995).

[50] J.K.Dickens, ORNL-9462, 6463(1988).

[51] G.G. Ohlsen, Nucl. Instr. Methods **37**, 240(1965).

[52] A.J. Koning, J.J. van Wijk and J.-P. Delaroche, "ECISVIEW: An interactive toolbox for optical model development", ECN report ECN-RX-97-046 (1997).

[53] S. Chiba, to be published.

[54] J.P. Delaroche, Y. Wang and J. Rapaport, Phys. Rev. **C39**, 391(1989).

[55] G. Hale, private communication (1997).

[56] F. Dietrich, private communication (1997).

[57] M. Kamimura and Y. Sakuragi, private communication, Dec. 1985.

[58] J.-P. Jeukenne, A. Lejune, C. Mahaux, Phys. Rev. **C15**, 10(1977)

[59] J.-P. Jeukenne, A. Lejune, C. Mahaux, Phys. Rev. **C16**, 80(1977)

[60] P.-G. Reinhard, "The Skyrme-Hartree-Fock Model of the Nuclear Ground State", Computational Nuclear Physics 1, Nuclear Structure, p.28, Springer-Verlag (1991).

Parameter	Set-1	Set-2
V_0	65.64	71.68
V_1	-26.71	-29.69
λ_v	0.00486	0.00495
r_v	1.34	1.22
a_v	0.707	0.822
W_{v_0}	10.19	10.06
W_{v_1}	18.42	14.03
W_{d_0}	74.69	321.4
W_{d_1}	15.69	18.76
λ_{W_d}	0.207	0.315
r_d	1.59	1.37
a_d	0.899	0.699
V_{so}	8.374	8.702
λ_{so}	0.01407	0.01407
r_{so}	1.58	1.64
a_{so}	0.427	0.311

Table 1: Optical potential parameters for n + ^{6}Li interaction

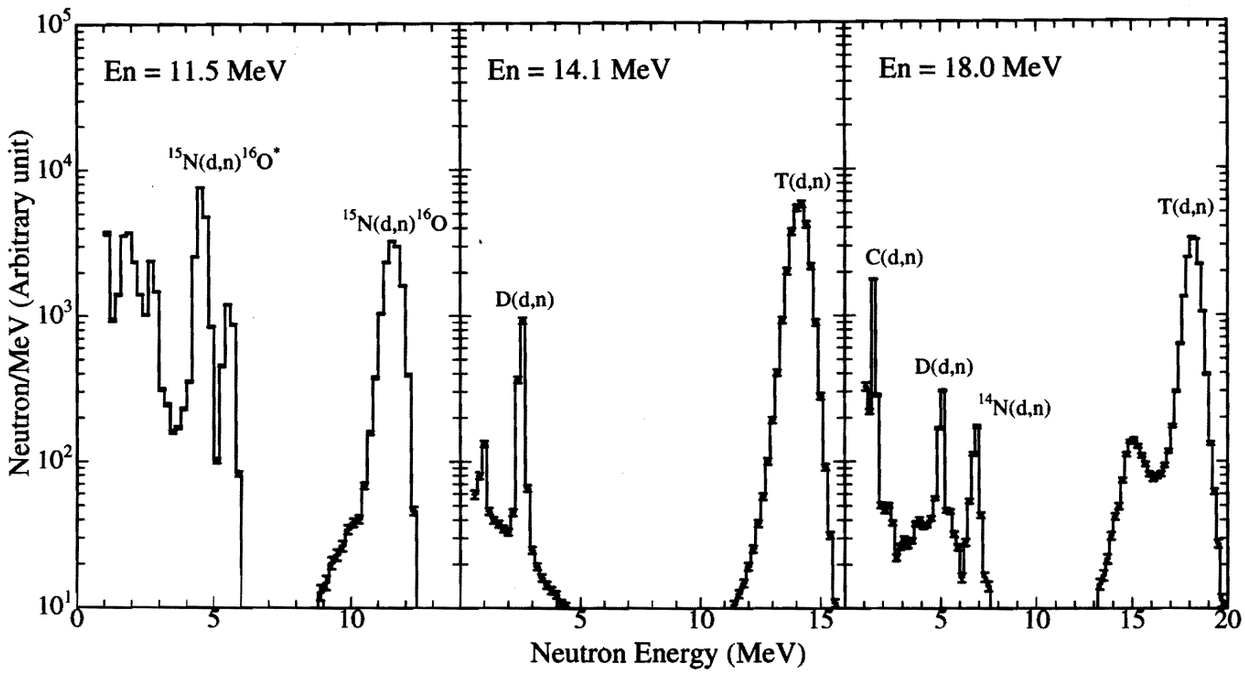

Fig. 1 Energy spectra of source neutrons for 11.5 (left), 14.1 (middle) and 18.0 (right) MeV experiments

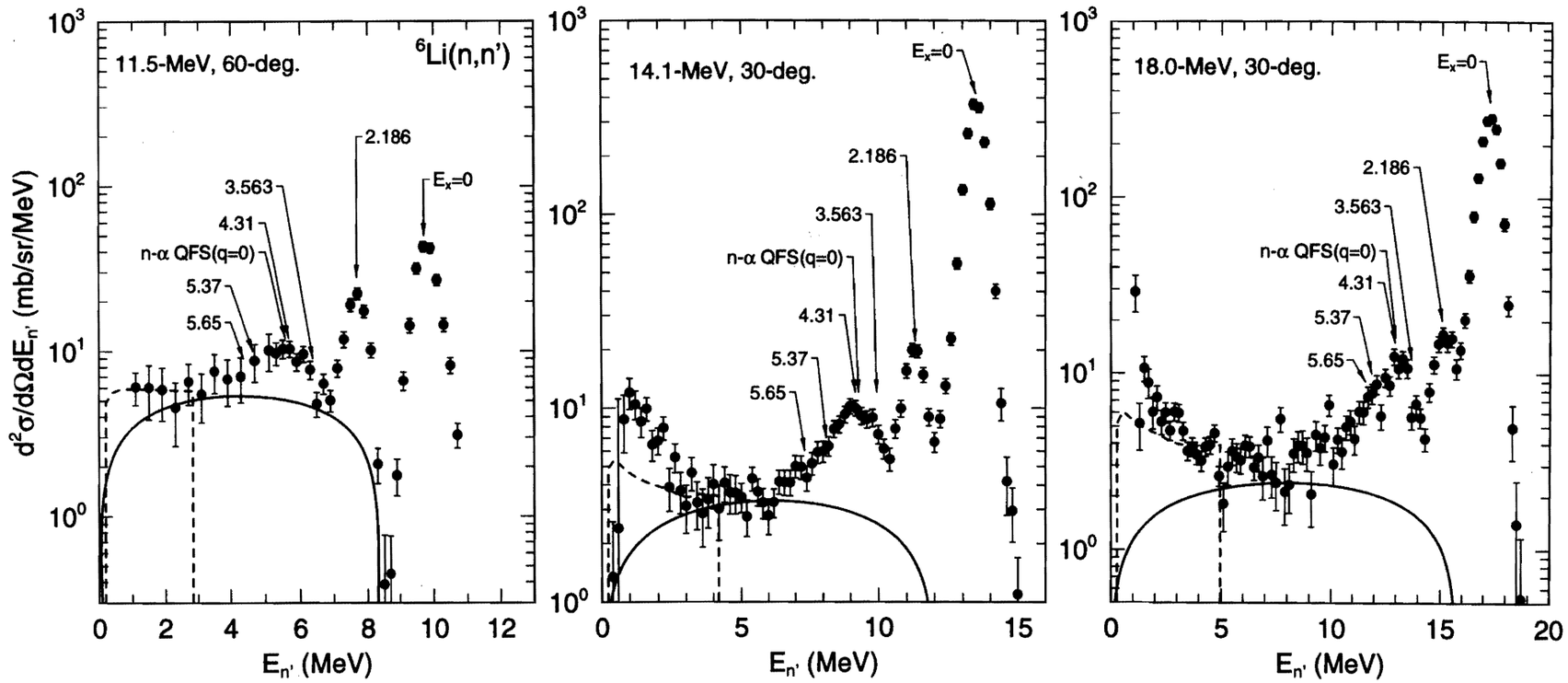

Fig. 2 Obserbed neutron energy spectra for projectile energy and emission angle of 11.5-MeV, 60-deg.(left), 14.1-MeV, 30-deg.(middle) and 18.0-MeV, 30-deg(right). The smooth curves show the 3-body phase-space factor, and the broken curves denote the spectra of neutron coming from the intermediate ^{5}He nucleus. Positions of neutrons corresponding to various excited states in ^{6}Li and n-α quasi-free scattering with 0 relative d-α momentum (q=0) are shown by arrows.

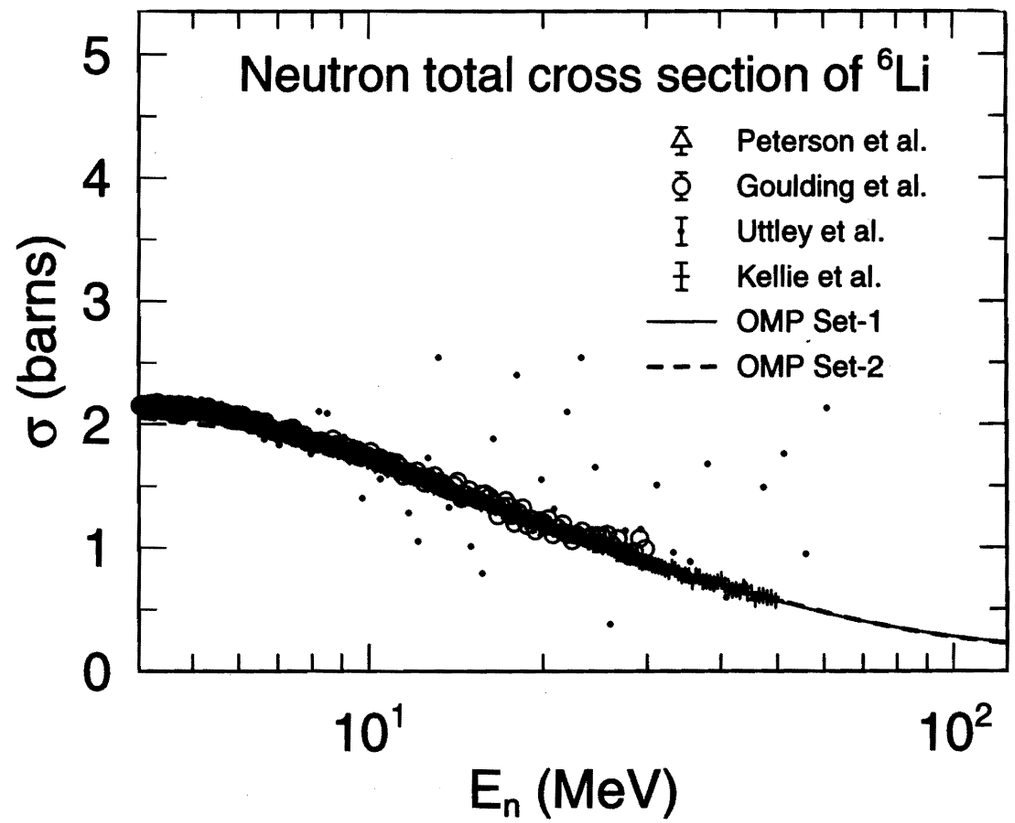

Fig. 3 Neutron total cross section of ^{6}Li. The 2 curves, marked as Set-1 and Set-2, denote the values calculated by the optical model with the potential set given in Table 1.

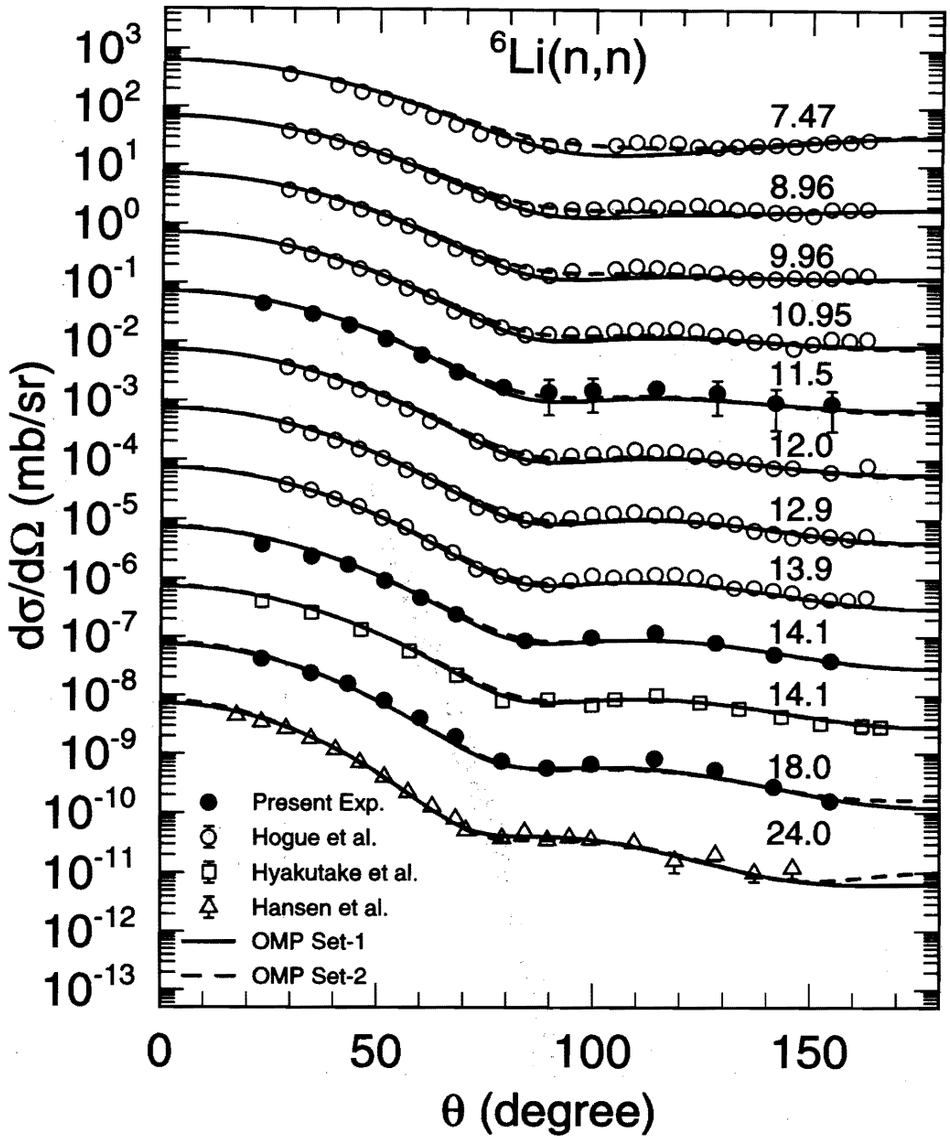

Fig. 4. Neutron elastic scattering angular distribution of ^{6}Li. The 2 curves, marked as OMP Set-1 and OMP Set-2, show the values calculated by the optical model with the potential sets given in Table 1. The numerical values denote the projectile energy in MeV. The data for 8.96, 9.96, ... were subsequently shifted downward by a factor of 0.1, 0.01, ..., respectively .

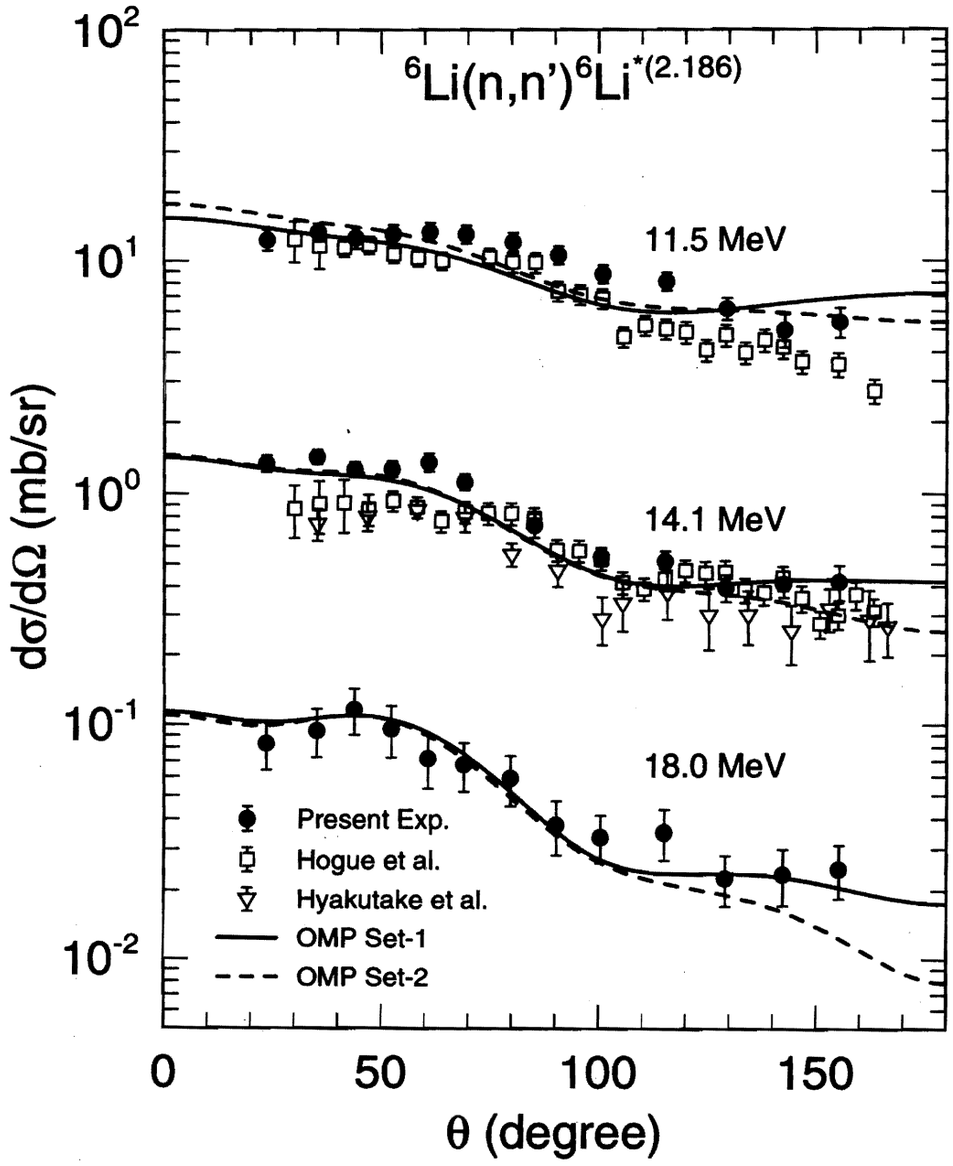

Fig. 5 Neutron inelastic scattering angular distribution to the 1st excited state of ^{6}Li. The 2 curves, marked as OMP Set-1 and OMP Set-2, show the values calculated by the optical model with the potential sets given in Table 1. The numerical values denote the projectile energy in MeV. The data for 14.1 and 18.0 MeV were shifted downward by a factor of 0.1 and 0.01, respectively.

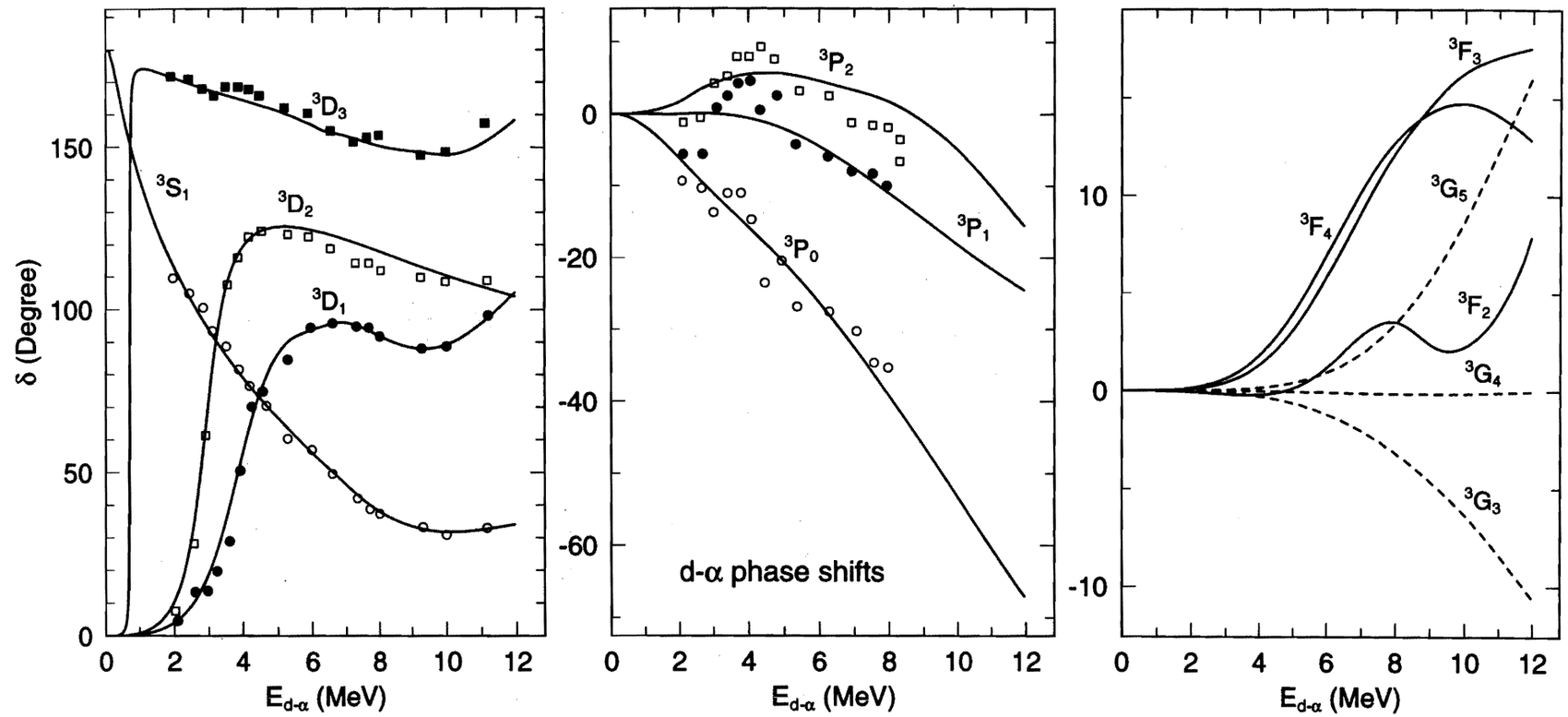

Fig. 6 The phase-shift data to reproduce the d-α elastic scattering. The curves were obtained by a R-matrix analysis of the ^{6}Li system. The symbols show the experimental data.

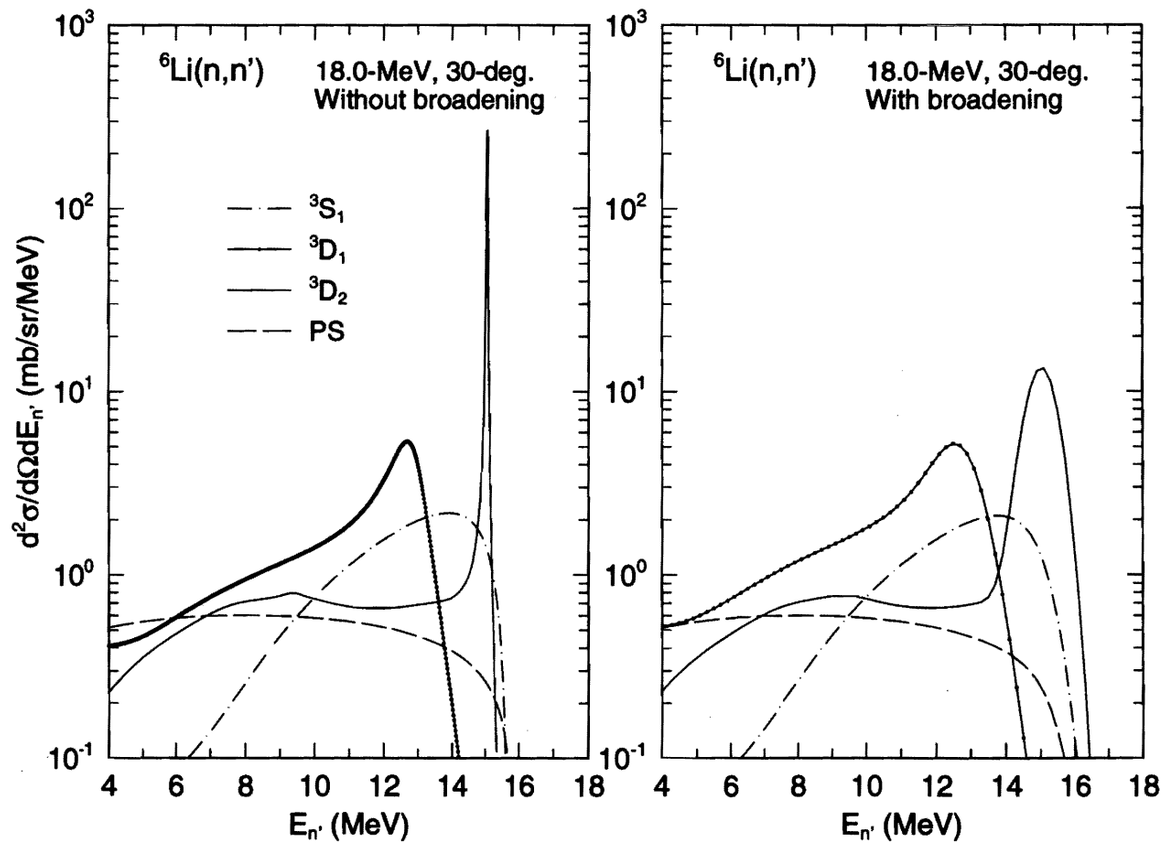

Fig. 7 Calculated continuum neutron spectra with (right) and without (left) the Gaussian broadening.

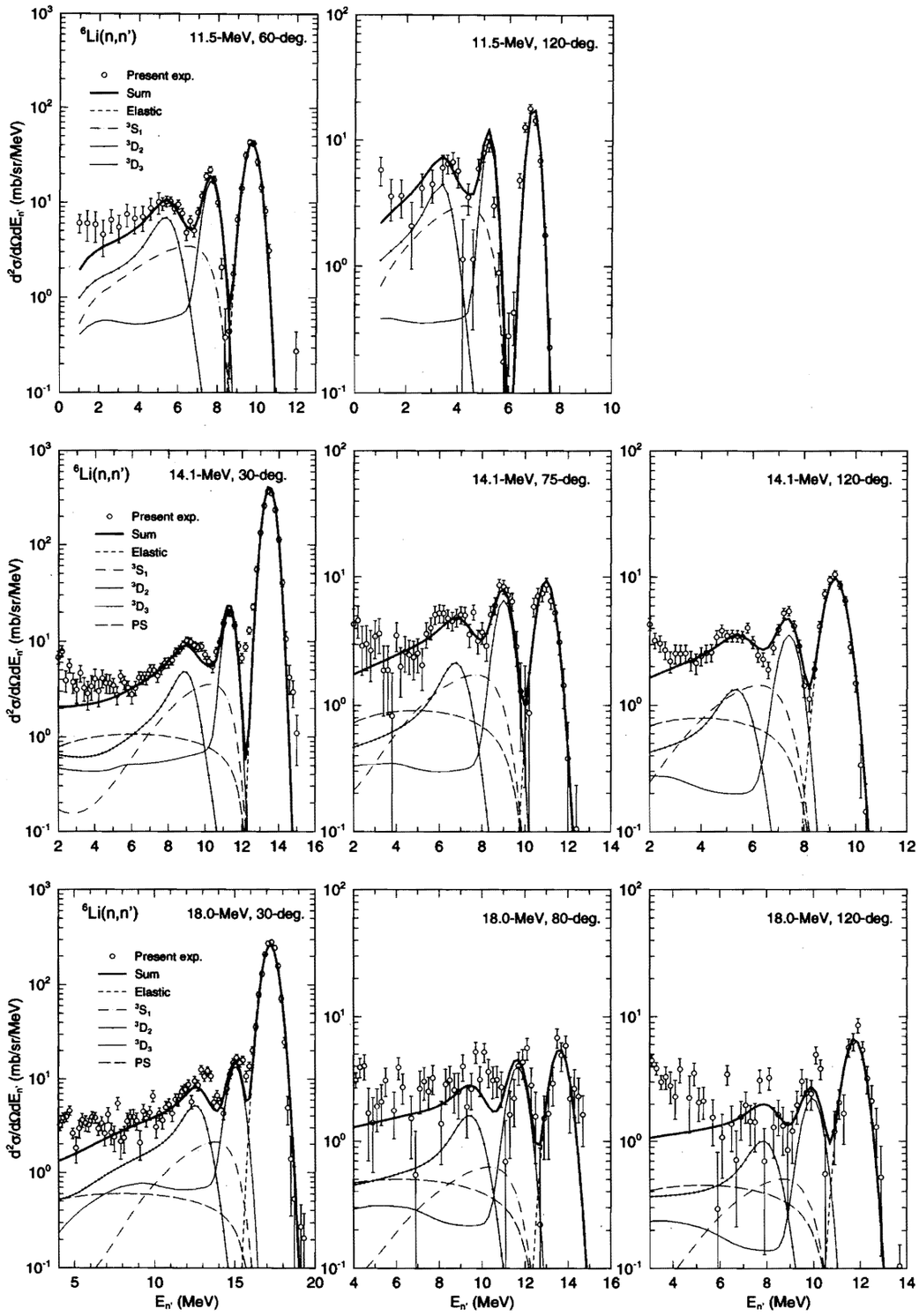

Fig. 8 Comparison of the neutron spectra calculated by the final-state interaction theory (as described in the text) and measured data at selected angular points.

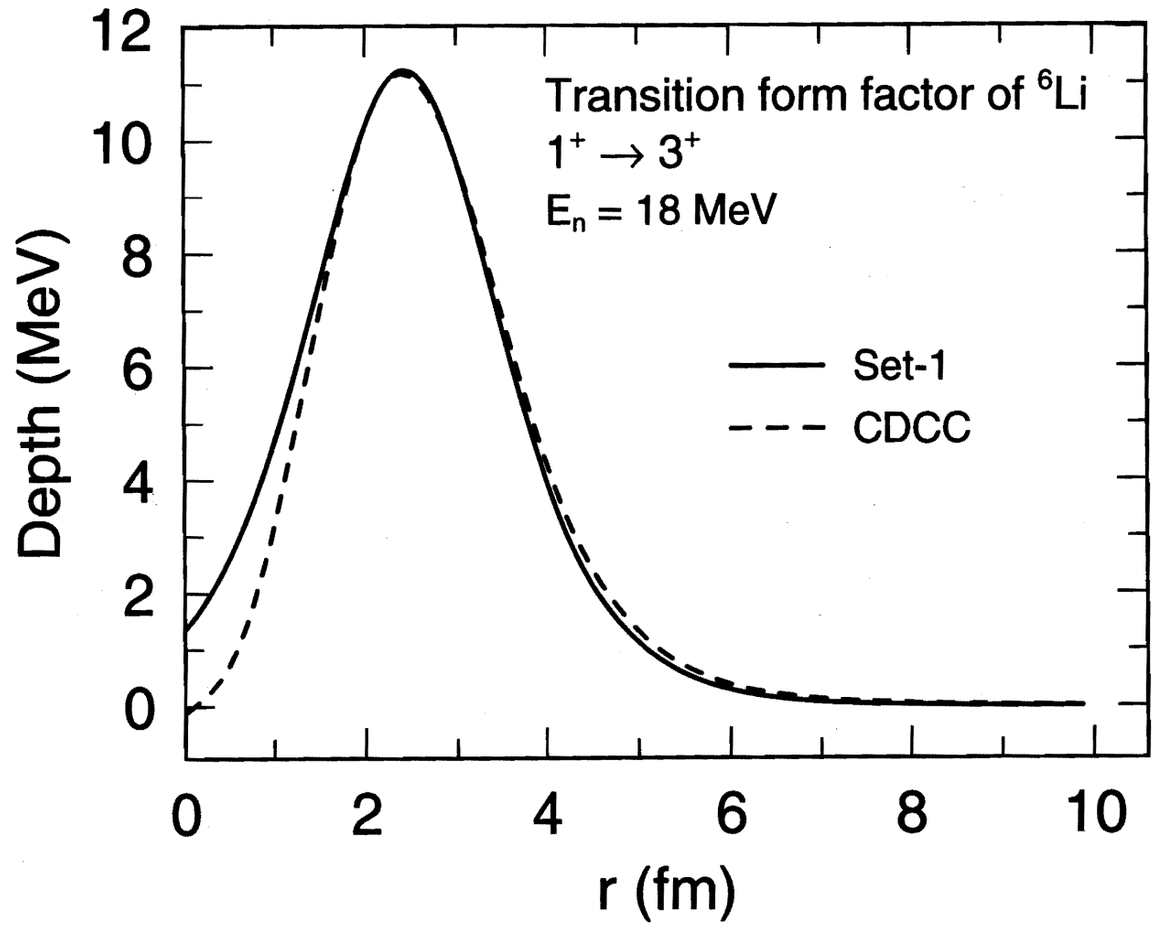

Fig. 9 Comparison of the transition form factor for the transition from the ground state to the 1st excited 3^+ state in ^{6}Li. The solid curve was obtained on the assumption of the macroscopic vibrational model (derivative of the Woods-Saxon potential) with the optical potential Set-1 in Table 1, while the broken curve was calculated by the fully-microscopic coupled-discretized continuum channel theory by Sakuragi et al.

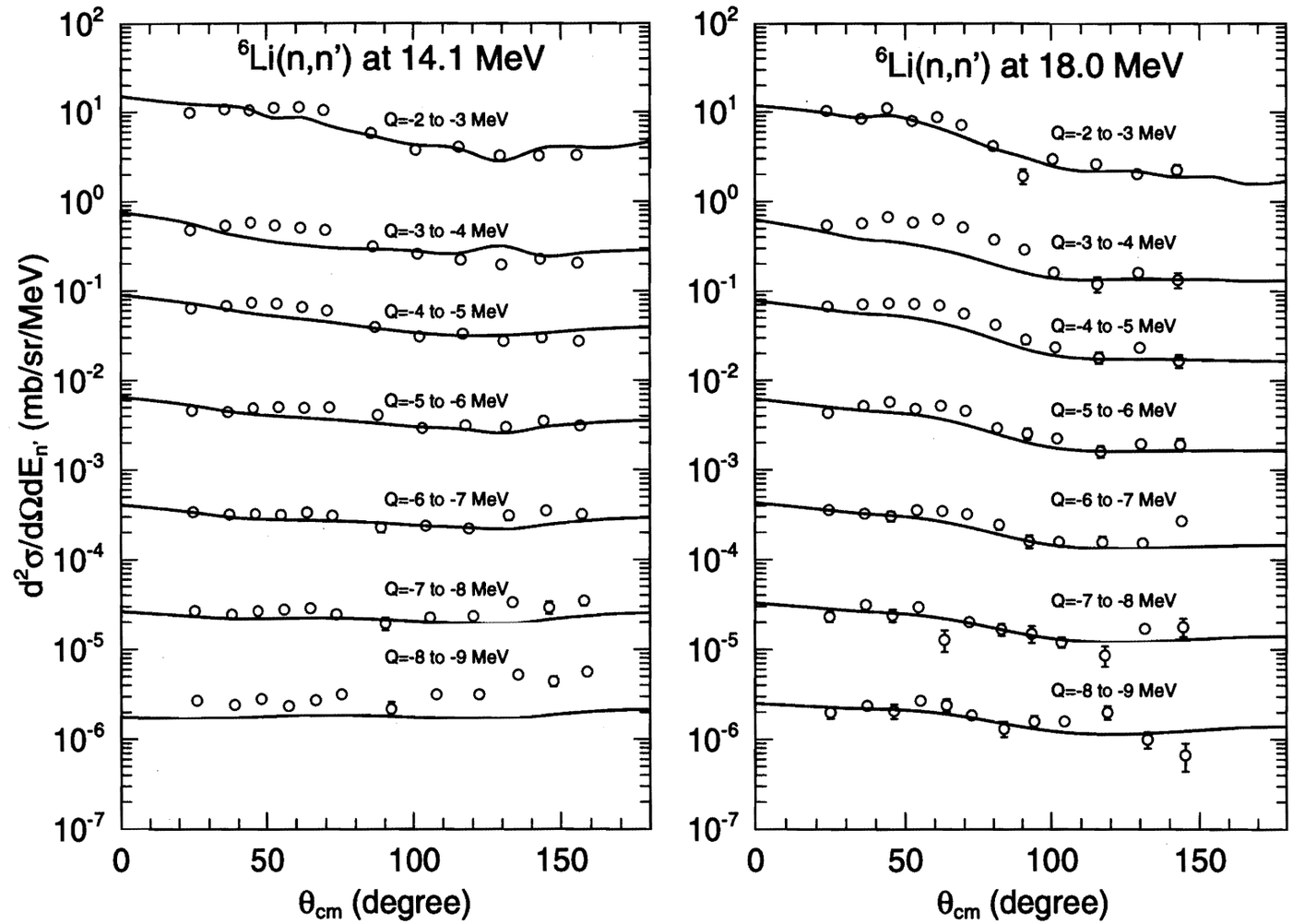

Fig. 10 Angular distributions of continuum neutrons for various Q-values bins at projectile energies of 14.1 MeV (left) and 18.0 MeV (right). The open circles show the experimental data, while the solid curves were calculated by the FSI theory. The data for Q=-3 to -4 MeV, -4 to -5 MeV, ... are shifted downward by a factor of 0.1, 0.01, ..., respectively.